Proceedings of the 17th World Congress
The International Federation of Automatic Control
Seoul, Korea, July 6-11, 2008

Robust Control of a High Precision 4-DOF Parallel Manipulator

Jacob W.F. Cheung*, and Y.S. Hung****

**Motion Control and Systems Laboratory, Research and Development Department, ASM Assembly Automation Ltd., 3/F Watson Centre, 16 Kung Yip Street, Kwai Chung, New Territories, Hong Kong. (e-mail: jacob.cheung@asmpt.com)*
***Department of Electrical and Electronic Engineering, The University of Hong Kong, Pokfulam Road, Hong Kong. (e-mail: yshung@eee.hku.hk)*

Abstract: A model-based robust control design approach is considered for a novel direct-drive 4-DOF parallel manipulator aimed at high speed and high precision semiconductor packaging applications. An experimental identification method is proposed to determine the dynamic model of the manipulator and a robust feedback controller is designed in the frequency-domain using genetic algorithm. Experimental results demonstrate that the motion performance of the 4-DOF parallel manipulator including positioning accuracy and steady-state error is improved significantly when compared with traditional XY, Z and θ motion stages. This shows that the proposed 4-DOF parallel manipulator provides a superior alternative to the traditional motion stages for high-precision motion.

1. INTRODUCTION

End-point accuracy, fast settling time and repeatability are essential for high-precision positioning mechanisms to assure product quality in the semiconductor packaging industry. In this paper, we propose a superior alternative to traditional XY, Z and θ motion stages for high-precision positioning, by means of a recently developed 4-DOF parallel manipulator under a model-based robust control scheme (Cheung, 2007). We verify our solution by means of an experimental prototype. Independent end-point position measurements are performed to show that the proposed system outperforms existing motion stages by a significant margin.

An experimental identification method is employed to determine the dynamic model of the parallel manipulator. Existing identification approaches include the measurement of motor input-output data and external force on the motion trajectory (Verdonck, Swevers, & Samin, 2001), application of Hamilton principle (Miller 1995) and the maximum-likelihood method (Olsen & Petersen, 2001). We will develop an identification approach using swept-sine method to excite the manipulator at different actuator positions such that the minimum plant gain at low frequency, the mechanical resonance and the gain and phase shift at high frequency can all be identified in the dynamic model. The feedback controller can then be designed using the model to ensure motion performance at the minimum plant gain while suppressing resonance and high frequency excitation to the manipulator.

Sage, de Mathelin & Ostertag (1999) has performed a survey of various robust control methods, such as acceleration feedback control (Chiacchio et al., 1993), computed-torque plus H_∞ control (Lee & Cheng, 1996; Lin & Brandt, 1998), nonlinear approach (Lim, Kang & Lee, 2000), μ-synthesis technique (Karkoub et al., 2000), fuzzy logic control (Choi, 2001) and variable structure control (Caballero, Armada & Akinfiev, 2004). In our proposed control design approach, an objective function is formulated to optimize the gain margin, phase margin, closed-loop control bandwidth and sensitivity to disturbance of the controller. The control parameters are designed using genetic algorithm such that a global minimum solution within the design criteria can be determined. It will be shown that the tracking response, robustness and sensitivity of the feedback controller within the desired closed-loop control bandwidth can be achieved using the proposed design method.

This paper is organized as follows. In Section 2, the kinematics model of the 4-DOF parallel manipulator is given and the dynamic model for system identification is described. The design of the robust controller is considered in Section 3. A prototype of the parallel manipulator has been constructed and the experimental setup of the prototype together with a high-precision laser displacement measurement system is described in Section 4. The results obtained from the experiments performed on the prototype are given in Section 5. Section 6 contains some concluding remarks.

2. KINEMATICS AND DYNAMIC MODEL

2.1 Kinematics model

Fig. 1 shows the kinematics design of the proposed 4-DOF parallel manipulator. The manipulator provides 3 DOF of translation in the XYZ space and 1 DOF in rotation against the Z-axis, and is driven by two linear miniature servomotor pairs located at (d_1,d_3) along the X-axis and (d_5,d_7) along the Y-axis. The linear actuators are coupled to two 2-DOF triangular planar mechanisms (referred to as a T-mechanism below) which are used to place the points $P(x_1,y_1)$ and $Q(x_2,y_2)$ at desired positions on the XY-plane. The small platforms at the outer joint of the T-mechanisms are

constrained by a belt mechanism to have only translational motion but not rotation on the XY-plane. Another T-mechanism is constructed on top of the platforms at the outer ends of the two T-mechanisms, with a 2-DOF rotational joint at each of the points *P* and *Q*. The third T-mechanism has motion restricted to a vertical plane. A platform mounted rigidly at the top of the vertical T-mechanism serves as the end-effector. The surface of the platform is constrained to the horizontal plane by a belt mechanism but can otherwise rotate about the Z-axis as the positions of *P* and *Q* are manipulated.

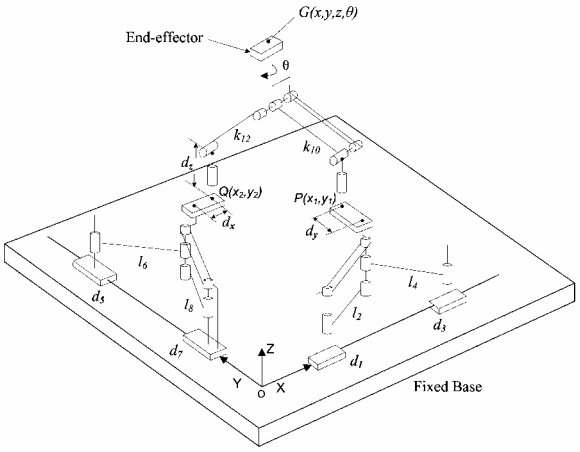

Fig.1. Kinematics design of the 4-DOF parallel manipulator.

Let the positions d_1, d_3, d_5 and d_7 satisfy the conditions

$$0<d_{1\min}\le d_1\le d_{1\max}<d_{3\min}\le d_3\le d_{3\max} \quad \text{and}$$
$$0<d_{7\min}\le d_7\le d_{7\max}<d_{5\min}\le d_5\le d_{5\max}. \qquad (1)$$

In the case when $l_2 = l_4 = l_6 = l_8 = l$ and $k_{10} = k_{12} = k$, the positions of P and Q are related to the actuator positions as

$$x_1 = \frac{1}{2}\left(d_1 + d_3\right), \quad y_1 = \sqrt{l^2 - \frac{1}{4}\left(d_3 - d_1\right)^2} + d_y,$$
$$x_2 = \sqrt{l^2 - \frac{1}{4}\left(d_5 - d_7\right)^2} + d_x \quad \text{and} \quad y_2 = \frac{1}{2}\left(d_5 + d_7\right) \qquad (2)$$

Then, the coordinates of the end-effector, denoted $G(x,y,z,\theta)$, are given by

$$x = \frac{1}{2}\left(x_1 + x_2\right), \quad y = \frac{1}{2}\left(y_1 + y_2\right),$$
$$z = \sqrt{k^2 - \frac{\left(x_2 - x_1\right)^2 + \left(y_2 - y_1\right)^2}{4}} + d_z \quad \text{and}$$
$$\theta = \tan^{-1}\left(\frac{y_2 - y_1}{x_2 - x_1}\right). \qquad (3)$$

For the inverse kinematics, we assume (by design of the workspace) that $x_1 > x_2$ and $y_1 < y_2$. Hence, (3) can be solved uniquely for $P(x_1, y_1)$ and $Q(x_2, y_2)$

$$x_1 = x + \sqrt{k^2 - \left(z - d_z\right)^2}\cos\theta,$$
$$x_2 = x - \sqrt{k^2 - \left(z - d_z\right)^2}\cos\theta;$$
$$y_1 = y - \sqrt{k^2 - \left(z - d_z\right)^2}\sin\theta, \text{ and}$$
$$y_2 = y + \sqrt{k^2 - \left(z - d_z\right)^2}\sin\theta. \qquad (4)$$

Under the conditions $d_3>d_1>0$ and $d_5>d_7>0$, the actuator positions can be solved from (2) as

$$d_1 = x_1 - \sqrt{l^2 - \left(y_1 - d_y\right)^2}, \quad d_3 = x_1 + \sqrt{l^2 - \left(y_1 - d_y\right)^2};$$
$$d_5 = y_2 + \sqrt{l^2 - \left(x_2 - d_x\right)^2}, \quad d_5 = y_2 + \sqrt{l^2 - \left(x_2 - d_x\right)^2}. \qquad (5)$$

2.2 Dynamic model

We will adopt a high order joint-space dynamic model of the 4-DOF parallel manipulator of the form

$$\frac{q_i(s)}{u_i(s)} = P_i(s) = L_i(s)\times H_i(s) \qquad (6)$$
$$L_i(s) = \frac{K_i}{s\left(s + \alpha_i\right)} \qquad (7)$$
$$H_i(s) = \prod_{m=1}^{M}\left(\frac{\omega_{im}^2}{\overline{\omega}_{im}^2}\right)\left(\frac{s^2 + 2\overline{\zeta}_{im}\overline{\omega}_{im}s + \overline{\omega}_{im}^2}{s^2 + 2\zeta_{im}\omega_{im}s + \omega_{im}^2}\right) \qquad (8)$$

where $q_i(s)$ (i = 1,3,5 and 7) is the position output of the translational joints, $u_i(s)$ is the controller input of the manipulator, $P_i(s)$ is the joint-space dynamic model of the manipulator, $L_i(s)$ is the low frequency model and $H_i(s)$ is the high frequency model of the manipulator, K_i is the system gain and α_i is the viscous friction coefficient of the translational joints, M is the number of resonant frequency included in the high frequency model, ω_{im} and $\overline{\omega}_{im}$ are the m^{th} resonant frequency and anti-resonant frequency of the translational joint i with the damping ratios ζ_{im} and $\overline{\zeta}_{im}$ respectively.

In the identification experiment, a low bandwidth motion trajectory is first selected to perform a point-to-point motion on the translational joints. The controller input and the translational joints position feedback are acquired to determine the model parameters of the low frequency model $L_i(s)$ expressed in (7) using prediction error method (PEM). The high frequency model $H_i(s)$ in (8) can be identified using the sweep-sine method. In this method, sinusoidal signal with desired peak amplitude over a specific frequency range is generated on the controller input to excite the mechanism. The translational joints acceleration is estimated from the encoder feedback position. The gain and phase of the high frequency model can be determined using the acceleration

output and the controller input of the translational joints. The high frequency model $H_i(s)$ in (8) is estimated using least square estimation (LSE) method.

3. ROBUST CONTROL DESIGN

A robust feedback controller is designed to control the position of the 4-DOF parallel manipulator as shown in Fig.2.

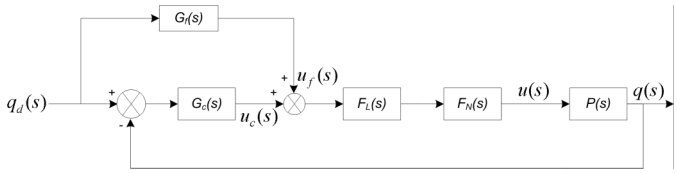

Fig.2. Block diagram of the robust controller.

The proposed control scheme consists of a PID controller $G_c(s)$, a lag compensator $F_L(s)$ and a notch filter $F_N(s)$ which can be expressed as

$$G_c(s) = \frac{u_c(s)}{e(s)} = \frac{\left(s^2 K_d + sK_p + K_i\right)}{\tau s^2 + s} \tag{9}$$

$$F_L(s) = \frac{K_L(s + f_c)}{(s + f_p)} \tag{10}$$

$$F_N(s) = \frac{s^2 + \sigma(\omega_h - \omega_l)s + (\omega_h \times \omega_l)}{s^2 + (\omega_h - \omega_l)s + (\omega_h \times \omega_l)} \tag{11}$$

where $u_c(s)$ is the PID controller output, $e(s)$ is the position error between the desired position $q_d(s)$ of the translational joint and the joint position $q(s)$ acquired from the linear encoder, τ is a time constant, K_L is the normalized gain of the lag compensator, f_p is the lower corner frequency and f_c is the higher corner frequency, σ is the attenuation of the notch filter measured from the resonant peak to the flat band of the plant gain with high break-frequency ω_h and low break-frequency ω_l.

The feedforward path of the proposed robust controller can be expressed as

$$\frac{u_f(s)}{q_d(s)} = G_f(s) = \left(K_j s^3 + K_a s^2 + K_v s\right) \tag{12}$$

where $u_f(s)$ is the control output of the feedforward path, K_v is the velocity feedforward constant, K_a is the acceleration feedforward constant and K_j is the jerk feedforward constant of the translational joint. Using the equations (9) to (12), the overall control law becomes

$$u(s) = F_L(s)F_N(s)\left(u_c(s) + u_f(s)\right) \tag{13}$$

Closed-loop stability, sensitivity to disturbance, robustness and fast tracking response are essential to the robust control design of the high-precision manipulator. Accordingly, the gain margin (*GM*), the phase margin (*PM*), the closed-loop control bandwidth (*CLBW*) and the sensitivity function (*S*) of the proposed robust controller are optimized to achieve the requirements of

$$GM = 20\log\left(\left.\frac{1}{\left|G_c F_L F_N P(j\omega)\right|}\right|_{\angle G_c F_L F_N P(jw) = -180}\right) \geq 7dB \tag{14}$$

$$PM = \angle G_c F_L F_N P(j\omega)\big|_{|G_c F_L F_N P(j\omega)|=1} \leq 60^\circ \tag{15}$$

$$CLBW = \min(\omega)\Big|_{\angle \frac{(G_c + FFC)F_L F_N P(j\omega)}{1 + G_c F_L F_N P(j\omega)} \leq -10^\circ} \geq 50Hz \tag{16}$$

$$\max\left|S(jw)\right|_{\omega \leq CLBW} = \max\left|\frac{1}{1 + G_c F_L F_N P(jw)}\right|_{\omega \leq CLBW} < 1 \tag{17}$$

An objective function is defined to be the gain margin difference ΔGM, phase margin difference ΔPM, closed loop bandwidth difference $\Delta CLBW$ and the maximum value of S over the *CLBW*, given by:

$$\begin{aligned} J(K_p, K_i, K_d, K_v, K_a, K_j, K_L, f_c, f_p, \sigma, \omega_l, \omega_h) \\ = \Delta GM + \Delta PM + \Delta CLBW + \max\left|S(j\omega)\right|_{\omega \leq CLBW} \end{aligned} \tag{18}$$

The control parameters of the proposed robust controller are then designed by solving the minimization problem of the objective function (18) using genetic algorithm.

4. PROTOYPE SETUP

The prototype of the 4-DOF parallel manipulator with a typical BGA substrate mounted on the end-effector to simulate the actual loading in semiconductor packaging operations is shown in Fig.3. The dimensions and the mechanical characteristics of the linkages are given in Table 1. The actual workspace of the 4-DOF parallel manipulator is about 35mm in *x*-axis, 35mm in *y*-axis and 6mm in *z*-axis. In Fig.3, a high precision laser displacement system with 0.91μm/mV resolution is mounted on the fixed base of the manipulator to provide an independent measurement of the end-effector position.

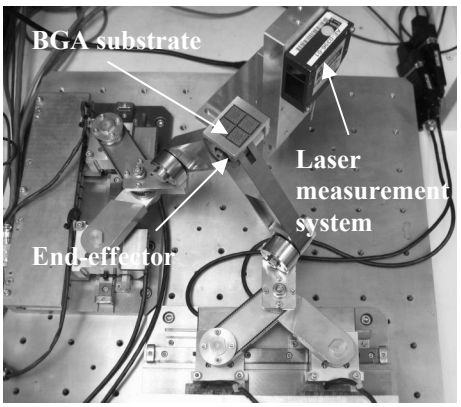

Fig.3. Experimental setup of the 4-DOF parallel manipulator.

Table 1. Kinematics and dynamics properties of the manipulator.

Parameter	Value
Actuator ranges (mm)	
d_{1min}, d_{7min}	59.5
d_{1max}, d_{7max}	99.5
d_{3min}, d_{5min}	119.5
d_{3max}, d_{5max}	159.5
Length (mm)	
l_2, l_4, l_6 and l_8	70
k_{10}, k_{12}	116.6
d_x, d_y and d_z	10
Mass (kg)	
m_1, m_3, m_5 and m_7	0.7
m_2 and m_6	0.104
m_4 and m_8	0.094
m_p and m_q	0.034
m_9 and m_{11}	0.019
m_{10}	0.147
m_{12}	0.13
End-effector m_{ef}	0.027
BGA substrate	0.0023

5. EXPERIMENTAL RESULTS

The joint based robust controller is designed using the dynamic model given in (6). The low frequency models are identified by PEM identification using two low speed motion trajectories of 5mm in 70ms for L_1 and L_3 and 4mm in 70ms for L_5 and L_7.The high frequency models H_1, H_3, H_5 and H_7 are determined by the swept-sine identification using a sinusoidal control signal with the frequency range from 80Hz to 500Hz to excite the mechanism. The frequency responses of the translational joints are acquired by placing the linear motor pair at different positions. The worst case frequency response of the translational joint with the lowest initial gain is selected for the controller design. The parameters of the robust controller of the 4-DOF parallel manipulator are then designed by using genetic algorithm and are listed in Table 2.

Table 2. Parameters of the robust feedback controller designed using genetic algorithm.

	d_1	d_3	d_5	d_7
K_p	0.7987	0.7229	0.9122	0.8438
K_i	0.003	0.001	0.0005	0.01
K_d	15.1038	12.8725	13.1532	15.4567
K_v	4.8751	5.5518	2.8185	9.6264
K_a	60.411	32.757	31.04	49.411
K_L	10	10	10	10
f_p (Hz)	305	316	320	305
f_c (Hz)	533	716	690	617
ω_r (Hz)	380	446	355	370
ω_b (Hz)	400	300	400	300
σ	15	25	15	30
GM (dB)	8.01	8.02	8.69	8.55
PM (deg)	50	50	49.3	60
CLBW	69.6	73.4	59.3	56.1
S	0.98	0.85	0.94	0.7

A motion trajectory is designed to carry out a point-to-point motion of the 4-DOF parallel manipulator for performing the substrate alignment process. The original location of the end-effector measured from the origin is (x_0, y_0, z_0, θ_0) = (91.4mm, 91.4mm, 123.7mm, -0.7854rad) and the destination is (x_1, y_1, z_1, θ_1) = (95.1mm, 96.9mm, 122.3mm, -0.8rad) with a target trajectory time of 70ms. The end-effector trajectory is mapped into four 5th order polynomial motion profiles for the linear actuators using the inverse kinematics model given in (4) and (5) and pre-computed in the PC. For the purpose of comparison, the PID computed-torque controller is evaluated along with the robust controller designed in section 3, and they are downloaded into the DSP platform for real-time control with sampling frequency of 2 KHz. The required end-point accuracy of the end-effector to the destination point is ±5μm in the XY plane, ±5μm in the vertical z-axis and ±0.2mrad in the θ-axis.

Figs. 4-7 show the position error of the actuators d_1, d_3, d_5 and d_7 as measured by the linear encoders in the joint space using the two different types of controllers. Table 3 demonstrates the improvement on the motion performance of the 4-DOF parallel manipulator. With the benefits of the proposed robust controller, the dynamic position error and the settling time of the linear actuators are reduced significantly compared to the traditional computed-torque control.

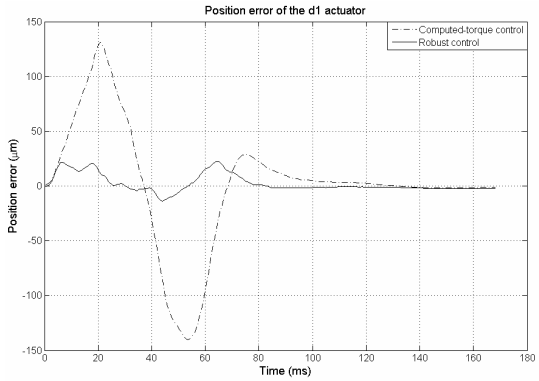

Fig.4. Position error of the d_1 actuator in the joint space.

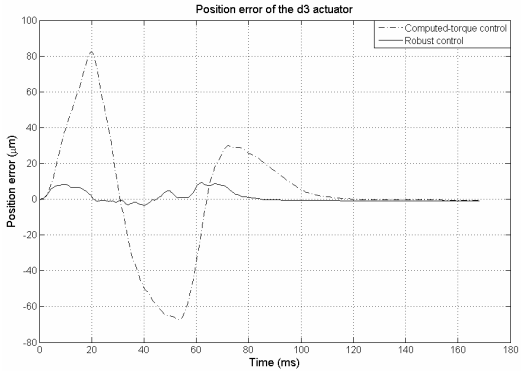

Fig.5. Position error of the d_3 actuator in the joint space.

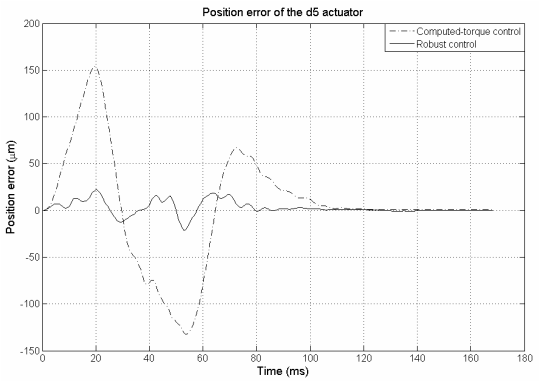

Fig.6. Position error of the d_5 actuator in the joint space.

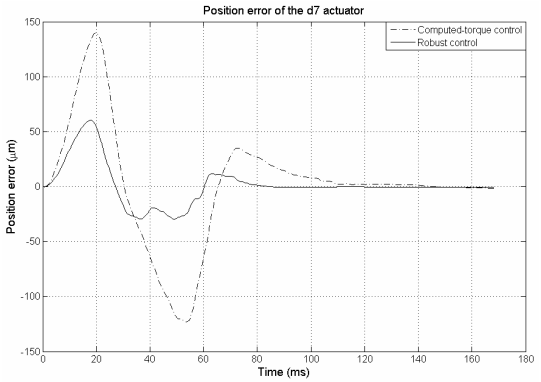

Fig.7. Position error of the d_7 actuator in the joint space.

Table 3. Motion performance improvement of the 4-DOF parallel manipulator using difference controllers.

	Computed-torque control	Robust control
Max. dynamic error of d_1 (μm)	140.2	22.4
Max. dynamic error of d_3 (μm)	82.2	9.2
Max. dynamic error of d_5 (μm)	154.0	22.2
Max. dynamic error of d_7 (μm)	140.2	47.0
Settling time of d_1 (ms)	30.0	5.0
Settling time of d_3 (ms)	30.5	3.0
Settling time of d_5 (ms)	34.0	8.0
Settling time of d_7 (ms)	34.0	3.0
Steady-state error of d_1 (μm)	-1.6	-2.4
Steady-state error of d_3 (μm)	-0.6	-1.0
Steady-state error of d_5 (μm)	0.8	-0.4
Steady-state error of d_7 (μm)	-1.6	-0.6

The end-point accuracy of the end-effector is verified independently using a laser displacement measurement system. The X, Y, Z and θ positions of the end-effector is measured over an interval covering the time when the position accuracy falls within ±5μm and the end of motion profile of the linear actuator. Figs. 8-11 show the settling response and the stead-state error of the end-effector using the robust controller (where the dotted vertical line corresponds to T_p =70ms). Table 4 shows that a significant improvement in the end-point positioning accuracy of the end-effector is obtained as compared with the traditional XY,Z and θ motion stage and the computed-torque controller.

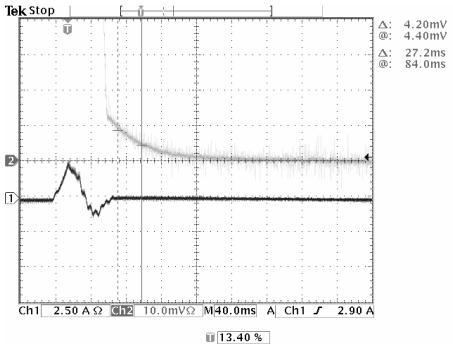

Fig. 8. Settling response of the end-effector in X-direction (grey) and the driving current (black).

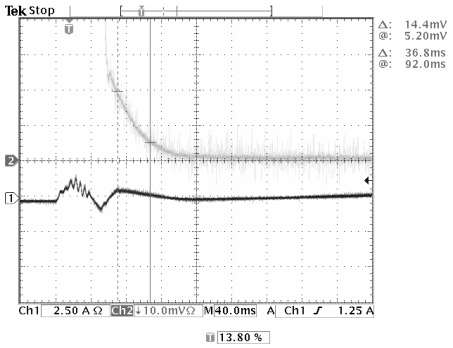

Fig. 9. Settling response of the end-effector in Y-direction (grey) and the driving current (black).

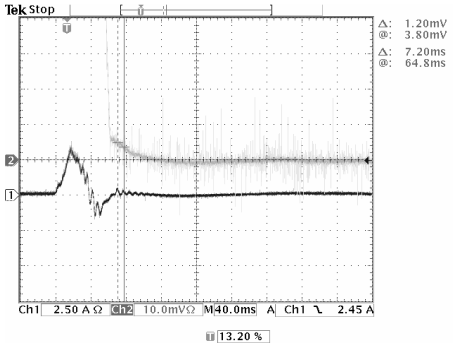

Fig. 10. Settling response of the end-effector in Z-direction (grey) and the driving current (black).

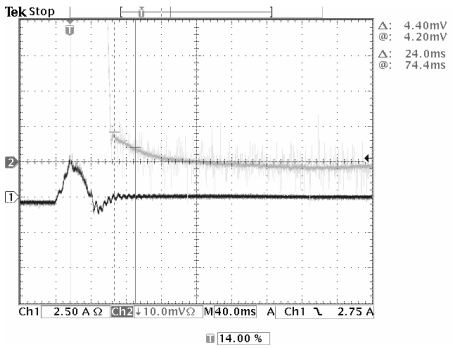

Fig. 11. Settling response of the end-effector in θ-direction (grey) and the driving current (black).

Table 4. Analysis of the settling time and end-point accuracy of the 4-DOF parallel manipulator using different controllers and the individual XY, Z and θ motion stage.

	XY, Z and θ motion stage (robust control)	4-DOF parallel manipulator (computed-torque control)	4-DOF parallel manipulator (robust control)
Settling time in X-dir (ms)	28	51.2	27.2
Settling time in Y-dir (ms)	22	49.6	36.8
Settling time in Z-dir (ms)	18	36.8	7.2
Settling time in θ-dir (ms)	23	54.4	24
End-point accuracy in X-dir (μm)	6.0	0	0
End-point accuracy in Y-dir (μm)	8.0	0.91	0.91
End-point accuracy in Z-dir (μm)	5.5	-0.91	0
End-point accuracy in θ-dir (μm)	4.8	-1.82	-1.82

From the results, the settling time of the 4-DOF parallel manipulator, in comparison with the individual XY, Z and θ stages under the same kind of robust feedback control scheme, has been reduced form 28ms to 27.2ms in X-direction and 18ms to 7.2ms in Z-direction, and the steady-state error has been reduced from 6μm to 0μm in X-direction and 8μm to 0.91μm in Y-direction, and 5.5μm to 0μm in Z-direction and 4.8μm to -1.82μm in θ-direction. These experimental results using independent laser measurement equipment demonstrated that the 4-DOF parallel manipulator under the proposed robust control scheme provides a superior alternative to the individual XY, Z and θ motion stages for high precision positioning.

6. CONCLUSIONS

A model-based robust control design approach is developed for a novel direct-drive 4-DOF parallel manipulator. A significant improvement in the end-effector steady-state error over the individual XY, Z and θ motion stages demonstrates the merits of the proposed parallel manipulator for high accuracy semiconductor packaging applications. The robust controller structure allows higher control gain to be used to improve the dynamic tracking performance of the manipulator without exciting the high-frequency resonant modes of the mechanism. The performance as measured by the high-precision laser displacement system provides an independent and convincing verification of the improvement in the end-effector positioning accuracy. This shows the effectiveness of the proposed control design method for the 4-DOF parallel manipulator. From the experimental results, the 4-DOF parallel manipulator provides a superior alternative to the use of individual XY, Z and θ motion stages for high-precision positioning applications.

REFERENCES

Caballero, R., Armada, M.A. and Akinfiev, T. (2004). Robust cascaded controller for nonlinearity actuated biped robots: experimental evaluation. *Int. J. of Robotics Research,* **23(10-11)**, 1075-1095.

Cheung, J.W.F. and Hung, Y.S. (2003). Kinematics optimization for high positioning accuracy of a 4-DOF parallel manipulator for semiconductor applications. In: *Proc. IEEE/ASME Int. Conf. on Advanced Intelligent Mechatronics*, pp.1256-1261, Kobe, Japan.

Cheung, J.W.F. and Hung, Y.S. (2005). Modelling and control of a 2-DOF planar parallel manipulator for semiconductor packaging systems. In: *Proc. IEEE/ASME Int. Conf. on Advanced Intelligent Mechatronics*, pp.717-722, Monterey, USA.

Cheung, J.W.F. (2007). *Kinematics, dynamics and control of high precision parallel manipulators*. Ph.D. Thesis, The University of Hong Kong.

Chiacchio, P., Pierrot, F., Sciavicco, L. and Siciliano, B. (1993). Robust design of independent joint controllers with experimentation on a high-speed parallel robot. *IEEE Trans. on Industrial Electronics*, **40(4)**, 393-403.

Choi, H.S. (2001). Robust control of robot manipulators with torque saturation using fuzzy logic. *Robotica*, **19(6)**, 631-639.

Karkoub, M., Balas, G., Tamma, K. and Donath, M. (2000). Robust control of flexible manipulators via μ-synthesis. *Control Engineering Practice*, **8(7)**, 725-734.

Kim, D.H., Kang, J.Y. and Lee, K.I. (2000). Robust tracking control design of a 6 DOF parallel manipulator. *J. of Robotic Systems*, **17(10)**, 527-547.

Lee, G.W. and Cheng, F.T. (1996). Robust control of manipulators using the computed-torque plus H_∞ compensation method. *IEE Proc. of Control Theory Appl.*, **143(1)**, 64-72.

Lin, F. and Brandt, R.D. (1998). An optimal control approach to robust control of robot manipulator. *IEEE Trans. on Robotics and Automation*, **14(1)**, 69-77.

Miller, K. (1995). Experimental verification of modelling of DELTA robot dynamics by direct application of Hamilton's principle. In: *Proc. IEEE Int. Conf. on Robotics and Automation*, pp.532-537, Nagoya, Japan.

Olsen, M.M. and Petersen, H.G. (2001). A new method for estimating parameters of a dynamic model. *IEEE Trans. on Robotics and Automation*, **17(1)**, 95-100.

Sage, H.G., de Mathelin, M.F. and Ostertag, E. (1999). Robust control of robot manipulators: a survey. *Int. J. of Control*, **72(16)**, 1498-1522.

Verdonck, W., Swevers, J. and Samin, J. (2001). Experimental robot identification: advantages of combining internal and external measurements and of using periodic excitation. *Journal of Dynamic Systems, Measurement and Control*, **123(4)**, 630-636.